Quantum Electronics **37** (4) 366 – 371 (2007)

INTERACTION OF LASER RADIATION WITH MATTER. LASER PLASMA PACS numbers: 52.50.Jm; 52.38.Mf; 81.07.–b; 61.43.Hv
DOI: 10.1070/QE2007v037n04ABEH013345

Formation of nanostructures upon laser ablation of a binary $Si_x(SiO_2)_{1-x}$ mixture

N.E. Kask, E.G. Leksina, S.V. Michurin, G.M. Fedorov

***Abstract*. The formation efficiency of fractal nanostructures is studied experimentally depending on the composition of the binary silicon – silica mixture during evaporation by millisecond laser pulse. The influence of percolation on the efficiency of nanostructure formation in a laser plume is discovered. It is found that the efficiency is maximal near the critical densities of atoms in the plasma, which correspond both to the three-dimensional and two-dimensional percolation. The dependences of the effective temperatures of the laser plasma and the intensity of spectral lines on the target composition are presented.**

Keywords: *laser ablation, laser plasma, percolation, nanostructures, fractals.*

1. Introduction

Synthesis of molecular nanostructures and the study of the process of their self-assembly into larger structures with unique properties and functions is a fundamental direction in the modern science. In the case of carbon, the variety of its allotropic forms leads to self-assembly of different nanoobjects – fullerenes and nanotubes. The synthesis of similar structures based on chemical elements belonging to the same subgroup of the periodic table seems promising. Special hopes are pinned on silicon, the element that follows carbon and has found wide applications in microelectronics [1].

One of the most promising methods for obtaining nanostructures is laser ablation, which allows the synthesis of nanostructures for many materials, including heat-resistant materials. Despite significant success of the method of laser ablation in the production of nanoclusters, the clear understanding of the mechanisms of their formation in the laser plasma has not been achieved so far. Usually, the model of a liquid drop, which is not applicable for structures containing less than several tens of atoms, is used. In this connection the important task is the proper consideration of branched molecular structures [2] and gas-like clusters [3] with a small number of atoms, because it is the atoms that are the nucleation centres. It was shown in [3] that in the dense plasma at high enough temperatures a gas-like cluster, representing a spontaneously appeared virtual chain of atoms, is realised with a greater probability than the close-packed structure. This model has not been confirmed experimentally yet.

Of interest is the study of the percolation model during the efficient formation of low-dimensional nanostructures in the dense plasma of the optical discharge. According to this model, when some critical density (percolation threshold) is exceeded, the corresponding component in the medium forms the so-called critical cluster of 'unlimited' length. The sizes of nodes and branches of a percolation cluster appearing in the vapour – gas region can change depending on the ratio of rates of nucleation and growth of elementary geometrical objects – compact and molecular clusters, as a rule, at a nanometer scale. In the limiting case of microscopic percolation [4], the thickness of branches of a percolation cluster can have atomic dimensions.

Previous studies of the emission spectra [5, 6] showed that three-dimensional percolation structures exist in plasmas produced upon ablation of targets into the surrounding gas by millisecond and nanosecond laser pulses. The percolation threshold is the critical atomic density of an evaporated component of the target. Upon laser ablation of one-component targets, percolation is manifested in the threshold dependences of the emission spectrum and the efficiency of formation of fractal nanostructures, when the density of the component particles changes with changing the external pressure produced by the buffer gas [7]. During the evaporation of binary targets, the dependence of emission on the component composition also has the threshold nature [8] (the corresponding measurements for the efficient formation of nanostructures have not been performed).

In this paper, we present the results of the experimental study of the formation efficiency of fractal nanostructures depending on the composition of the binary silicon – silica mixture evaporated by millisecond laser pulses.

According to [9], upon ablation of a silicon target containing silica impurity, a layer of silicon monoxide is formed on which nanowires of crystal silicon are produced and grow. The efficiency of the process is maximal when the weight fractions of the components (silicon and silica) in the target are the same, and substantially exceeds the growth efficiency typical for the known vapour – liquid – solid (VLS) mechanisms [10]. The growth of the nanowires according to the VLS model occurs in the region of its contact with the

N.E. Kask, E.G. Leksina, S.V. Michurin, G.M. Fedorov D.V. Skobel'tsyn Research Institute of Nuclear Physics, M.V. Lomonosov Moscow State University, Vorob'evy gory, 119992 Moscow, Russia;
e-mail: nek@srd.sinp.msu
Received 14 July 2006

Kvantovaya Elektronika **37** (4) 366 – 371 (2007)
Translated by I.A. Ulitkin

liquid drop of a nanometer size, which apart from silicon also contains impurity metals (Au, Fe, Ni, Co). The composition of the produced melt is close to the composition at the eutectic point, and the balance of the matter is provided by the supply of atoms of saturated vapour. One-directional growth of nanowires occurs when the drop is in the vapour whose temperature is one hundred – two hundred degrees lower than the temperature of the epitaxial deposition of the matter (for silicon, $T \sim 1150\,^{\circ}\mathrm{C}$).

2. Experimental

The scheme of the experimental setup is presented in [7]. A neodymium glass laser consisted of a master oscillator and an amplifier. The quasi-continuous regime was obtained by using a nearly concentric resonator in the master oscillator. It provided a comparatively low ($\sim 15\,\%$) modulation depth of the generated power in the frequency range from 10^4 to 10^7 Hz. The target was evaporated under the action of a ~ 10-ms FWHM bell-shaped laser pulse. The laser pulse energy was varied with neutral light filters in the range from 10 to 100 J. The laser radiation was focused on the target by a spherical lens with the focal length of 300 mm into a spot of diameter ~ 1 mm. The flow density on the target surface equal to $\sim 10^5$ W cm^{-2} corresponded to the maximum efficiency of the nanostructure formation. The decrease in the efficiency at a higher density is obviously related to the destruction of fractal aggregates by laser radiation.

The sample under study was placed in a sealed chamber with the diameter and length of the internal cavity of 25 and 150 mm, respectively. The pressure of the inert buffer gas (Ar or He) was 1 or 30 atm. According to [7], the majority of materials, including silicon, form most efficiently fractal nanostructures at pressures close to normal. At a pressure of 30 atm the threshold of fractal shell formation is exceeded [7]. The target was a mixture of silicon and silica powders with the grain size of about 10 μm, pressed at a pressure of 60 atm. The fine-dispersed phase produced in the laser plume was deposited on a glass substrate placed horizontally on the chamber bottom.

To separate structures, which are formed by the laser pulse and are deposited on the substrate within several seconds after its end, we pumped out the buffer gas containing the fine-dispersed phase. If the gas is not pumped out, the nearly complete deposition of fractal microclusters and formation of a layer on the substrate terminated within 15 min after the laser pulse action. The optical density of the layer, determined by the intensity of the transmitted or scattered probe radiation from an incandescent lamp characterised the formation efficiency of fractals. Photographs of the layers were processed with the standard Adobe PhotoShop programs.

We also studied the spectrum and intensity of the laser plasma emission propagating in two directions: longitudinal (towards the laser beam) and transverse (perpendicular to the plume axis). In the latter case, the emission of the plasma layer at a distance of 500 μm from the target surface was studied by using a spectral attachment with a diffraction grating from a VFU-1 setup. The spectrum was recorded with a CCD array (3650 pixels) every 3 ms. Spectra were studied in the wavelength range from 350 to 650 nm with a resolution of 0.08 nm. In the longitudinal direction, the emission of the total volume occupied by plasma was directed to the entrance of a SFL-451 spectrofluorimeter operating in the wavelength range from 400 to 900 nm with a resolution of 6.4 nm. The effective colour and brightness plasma temperatures were determined by comparing the emission intensities of the plume and a reference SI8-200U tungsten band lamp. To eliminate the effect of the geometrical factor during calibration measurements, the reference source was placed instead of the target.

3. Experimental results

3.1 Formation of fractal nanostructures

Figures 1 and 2 show the experimental dependences of the efficiency of nanostructure formation on the target composition (on the weight fraction x of silicon in the target and the relative density n_{Si} of silicon atoms in the plasma) in the buffer gas at pressures of 30 and 1 atm. Under the assumption that upon ablation the relative content of evaporated components of the target does not change and the complete thermal decomposition (dissociation) of molecules occurs, the expression

$$n_{\mathrm{Si}} = \frac{x\mu_{\mathrm{SiO_2}} + (1-x)\mu_{\mathrm{Si}}}{x\mu_{\mathrm{SiO_2}} + 3(1-x)\mu_{\mathrm{Si}}} \tag{1}$$

is valid for the relative density of silicon atoms in the plasma. Here, μ_{Si} and $\mu_{\mathrm{SiO_2}}$ are molecular weights of the target components. (Note that $n_{\mathrm{O}} = 1 - n_{\mathrm{Si}}$ for the relative density of oxygen atoms. The values of n_{Si}, corresponding to the weight fraction x, are shown at the upper scale of Fig. 1.)

Because the density of heated fractal structures suspended in the chamber volume approaches the buffer gas density, the comparison of the efficiencies of gases under study may prove incorrect. Thus at a pressure of 30 atm, the density of the ablation cloud is smaller than that of argon but higher than the helium density. As a result, nearly all the structures were deposited in helium, whereas in argon they condensed at the top of the chamber. Only the heaviest

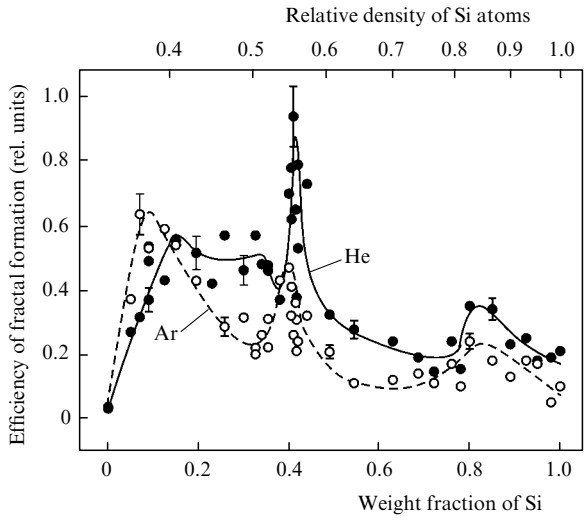

Figure 1. Experimental dependences of the formation efficiency of nanostructures on the target composition in the buffer gas (He, Ar) at a pressure of $p = 30$ atm. The time of the layer deposition is 15 min.

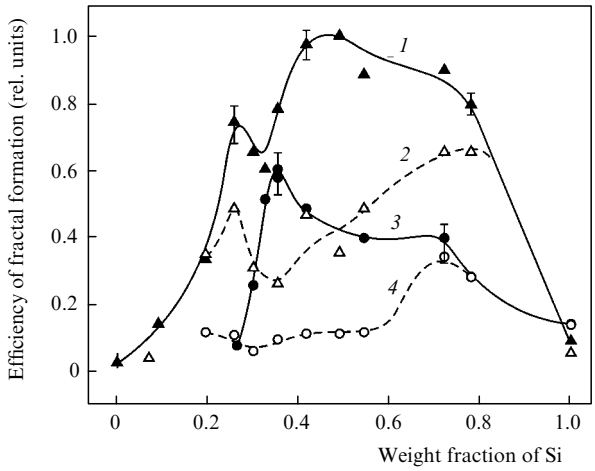

Figure 2. Experimental dependences of the formation efficiency of nanostructures on the target composition in the buffer gas (Ar) (*1*, *2*) and (He) (*3*, *4*) for $p = 1$ atm; measurements were performed 15 min after the laser action (*1*, *3*) and immediately after the action (*2*, *4*).

aggregates with the fractal dimensionality of $d_f > 2$ descended. The layer formed by them within 5 s after the end of the laser pulse had $d_f \sim 1.71 \pm 0.06$ (Fig. 3). Fractals consist of compact nanoparticles with the characteristic size of 80 nm. Branched structures with $d_f \sim 1.43 \pm 0.12$ prevail in the layer deposited in helium. The value of d_f of fractals deposited in argon but at a pressure of 3 atm is close to the value of d_f of fractals deposited in helium. In this case the argon density is approximately equal to the helium density at a pressure of 30 atm. (Note that the fractal dimensionality d_f for structures on the substrate was calculated by the cell method.)

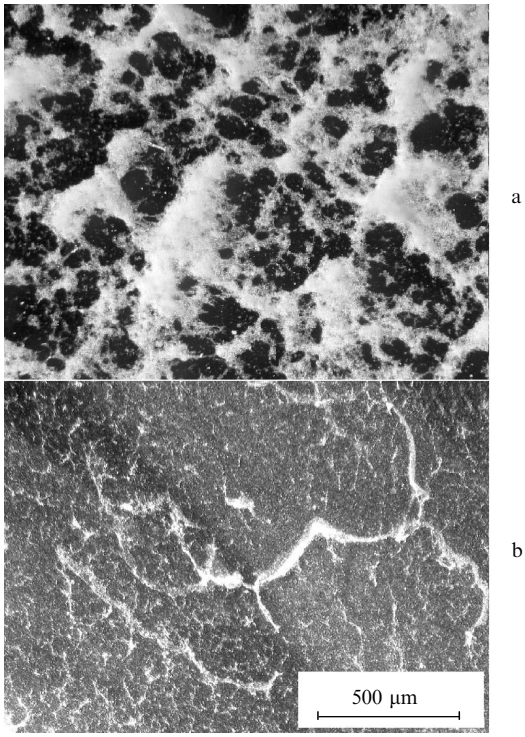

Figure 3. Fractal layer formed on a substrate within 5 s after the laser pulse end at a 30-atm pressure of the Ar (a) and He (b) buffer gases.

If the pressure of the buffer gas is 1 atm, all the structures collected at the cell bottom both in helium and argon. It follows from a comparison of dependences presented in Fig. 2 that at a normal pressure, the efficiency of structure formation in argon is several times higher than in helium. The behaviour of the dependences near the two-dimensional percolation threshold is explained by the difference of ejecting forces acting on the fractals. The two-dimensional percolation is realised in the medium with the same density of components (in the plasma under study, with equal density of silicon and oxygen atoms). One can see from Fig. 1 that a well pronounced narrow peak is observed in the region of compositions $x \approx 0.41$ ($n_{Si} \approx 0.55$) at a helium pressure of 30 atm, while in argon a large scatter of experimental points is observed which can be treated as a narrow dip in a broad peak.

At the buffer gas pressure of 30 atm, fractal macrostructures – fractal shells (according to the terminology in [7]) are formed, which appear during the laser pulse at the periphery of the plasma region. Fragments of shells of size 1 – 10 mm are observed in a wider range of compositions ($0.1 < x < 0.9$). Figure 4 shows a microphotograph of such a two-dimensional structure, which resembles a transparent folded fabric. The formation of shells, which 'emerge' in the argon atmosphere, do not deposit on the substrate and do not contribute to the thickness of the deposited layer, also results in an apparent decrease in the efficiency of fractal formation.

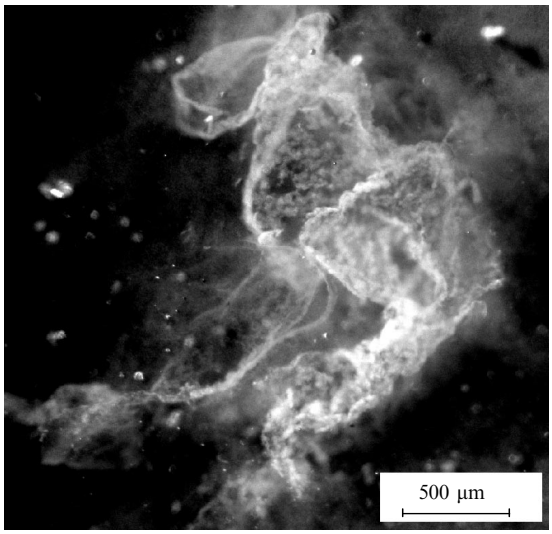

Figure 4. Fractal shell. Weight fraction of silicon $x = 0.326$; buffer gas – He, $p = 30$ atm.

3.2 Effect of the target composition on the optical spectrum and the effective temperatures of the laser plasma

It was established in [7] that during the evaporation of many materials under the action of quasi-continuous laser radiation, the intensity of the plume emission drastically increases by several orders of magnitude at some external pressure, whose value is determined mainly by the target material. It was assumed in [7] that at a threshold pressure of the surrounding gas, the interaction energy of dispersed-

phase particles in the laser plasma becomes equal to their kinetic energy. As a result, a disordered macroscopic fractal structure appears in external layers of plasma already during the action of laser radiation. In this case, the absorptivity and emissivity of plasma and the effective colour temperature, describing the spectrum continuum of the light flash, noticeably increase. According to [6], the increase in the continuum intensity is accompanied by a decrease in the intensity of discrete atomic and ionic spectra, because atoms and ions entering the composition of the percolation cluster do not contribute to discrete spectra. The spectra of emission propagating in the direction perpendicular to the laser beam axis were studied in [5]. The fractal shell produced around the plasma plume can decrease the emission intensity in this direction. The laser radiation prevents the formation of fractal shells at the leading edge of the plume.

Figure 5 shows the dependences of the effective colour temperature on the composition of the target. In the longitudinal direction, the colour temperature of plasma in argon exceeds the emission temperature in helium by 20 % on average. In the spectral interval under study, the experimental values of the effective brightness temperature coincide with the effective colour temperature within 15 % of the measurement error, which indicates the absence of strong absorption at the leading edge of the plume. The emission in the transverse direction has the same colour temperature as in the longitudinal direction. The difference between the brightness and colour temperatures in the transverse direction depends both on the mixture composition and on the distance between the plasma layer under study and irradiated surface of the target. The fine-dispersed condensed phase (fractal shell) accumulating at the plume periphery reduces the emission intensity near the target by two – three orders of magnitude (in argon by an order of magnitude stronger than in helium).

The dependences of the intensity of spectral lines in plasma on the target composition are shown in Figs 6 and 7. The dependences are presented for typical lines of silicon ions (SiII, $\lambda = 634.7$ nm), oxygen atoms (OI, $\lambda = 777.1$ nm) and molecules (O_2, the primary atmospheric absorption band at $\lambda = 759.6$ nm) and atoms of sodium (NaI, D line, $\lambda = 590.0$ nm) and calcium (CaI, $\lambda = 396.8$ nm), which are used as impurities to the silicon powder in the target composition. To take into account changes from pulse to pulse in the absorbing layer and the changes in the target composition, the line intensities in Figs 6 and 7 are normalised to the continuum intensity in the corresponding spectral region. The results presented for SiII ions and Na and Ca atoms were obtained for the plasma emission in the transverse direction and for oxygen – in longitudinal direction.

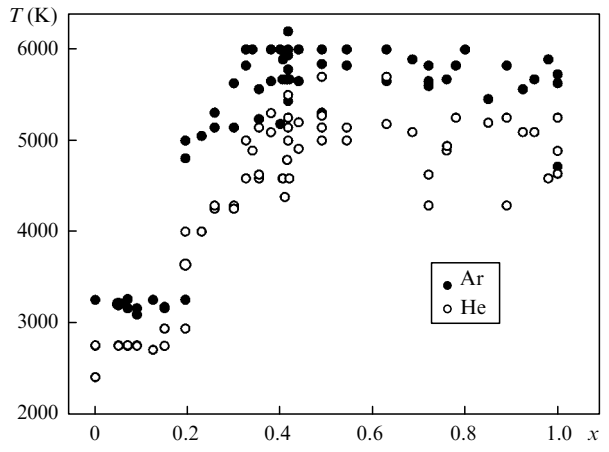

Figure 5. Dependences of the effective colour temperature of plasma emission on the target composition at a buffer gas (Ar, He) pressure of 30 atm.

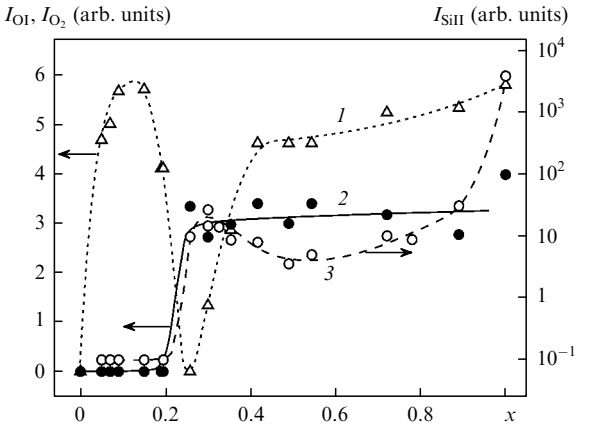

Figure 6. Dependences of the spectral line intensities of atomic oxygen at 777.1 nm (*1*), molecular oxygen at 759.6 nm (*2*) and silicon ion at 634.7 nm (*3*) on the target composition; buffer gas is helium, $p = 30$ atm.

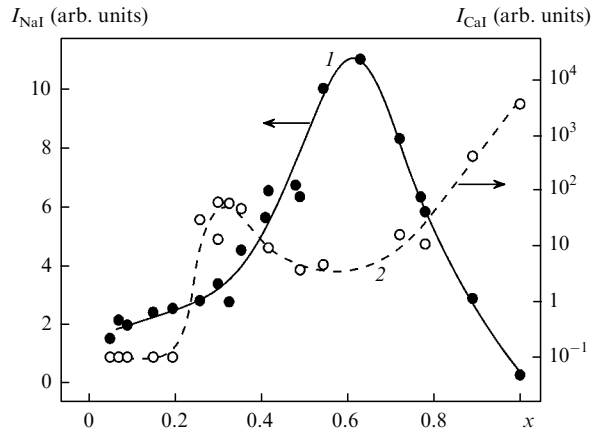

Figure 7. Dependences of the spectral line intensities of NaI at 590.0 nm (buffer gas is helium, $p = 30$ atm) (*1*) and of CaI at 396.8 nm (buffer gas is argon, $p = 30$ atm) on the target composition.

4. Discussion of the results

At constant pressure and temperature, the equilibrium constant k_{eq} of evaporation processes and thermochemical decomposition is determined by the change in the Gibbs energy [11]:

$$-RT\ln k_{eq} = \Delta G = \Delta H - T\Delta S, \qquad (2)$$

where ΔH and ΔS are changes in enthalpy and entropy during the reaction and R is the gas constant. The

beginning of the spontaneous process (chemical boiling) is determined by the equality $\Delta G = 0$.

According to [12], the spontaneous decomposition of silica at a normal pressure occurs in the reaction

$$SiO_2(c,l) \leftrightarrow SiO(g) + \frac{1}{2}O_2(g) \quad (3)$$

at temperature $T_r^0 = 3050 \pm 70$ K with the thermal effect $\Delta H_r^0 = 171$ kcal mol^{-1} and the entropy change $\Delta S_r^0 = 54.2$ cal mol^{-1} K^{-1}.

For the silicon monoxide, the displacement of the reaction equilibrium

$$SiO(g) \leftrightarrow Si(g) + O(g) \quad (4)$$

to the thermal decomposition at a normal pressure occurs at temperature $T \approx 6000$ K [13].

Thermochemical calculations presented in [14] indicate that already at temperature 3100 K nearly all silica particles are decomposed into monoxide and molecular oxygen according to reaction (3) (concentration of other components in the plasma can be neglected). As the temperature increases to 5000 K, the molar concentration of SiO does not change and the molecular oxygen partially dissociates.

As follows from the results of [15], a substantial change in the threshold temperatures in the case of spontaneous decomposition of silicon oxides does not occur at a pressure of 30 atm. It follows from Fig. 5 that the plasma temperature does not exceed 3200 K for the mixture composition $0 < x < 0.2$. As a result, the silicon dioxide is decomposed according to reaction (3). At this temperature, reaction (4) is directed to the formation of silicon monoxide. Therefore, free silicon atoms are absent, which agrees with the results of the experiment (see. Fig. 6). When targets with $0.23 < x < 1$ are evaporated, the plasma temperature exceeds 6000 K (see Fig. 5), the reaction direction shifts to the SiO molecule decomposition and lines of silicon ions are present in the emission spectrum (see Fig. 6).

The threshold changes in the temperature and intensity of spectral lines belong to the target composition with $x = 0.23 \pm 0.03$. The volume fraction of silicon in the target is

$$p_V = \left(1 + \frac{\rho_{Si}(1-x)}{\rho_{SiO_2} x}\right)^{-1}$$

(ρ_{Si} and ρ_{SiO_2} are the densities of silicon and silica) for this x is close to the threshold one ($p_V^{th} \approx 0.33$) for the three-dimensional percolation according to the model of overlapping spheres. The formation of a percolation cluster from silicon particles in the target volume does not lead to a drastic increase in the laser radiation absorption, for example, at low enough pressures ($p < 3$ atm) of the buffer gas. It is obvious that such a high value of temperature ($T \sim 6000$ K), which is observed for $x > 0.3$, cannot be provided only by absorption in the plume plasma. According to [7], when the target is irradiated by millisecond laser pulses, its surface is heated to the boiling point of the material. The temperature in the laser plume in the regime of developed evaporation does not differ substantially from it if the pressure of the buffer gas is lower than some value typical for materials of the target.

The absorption bands of molecular oxygen are observed only upon ablation of targets with the silicon concentration exceeding the threshold value. Oxygen molecules, absorbing radiation of central layers of the plasma plume with temperature ~ 6000 K, reduce the radiation intensity of the maximum of the band by two–three times, by decreasing the effective brightness temperature by no more than thousand degrees. The absence of the absorption spectrum of molecular oxygen and vice versa the presence of the emission spectrum of its atoms for compositions lower than the threshold one ($x < 0.23$) cannot be explained within the considered model.

Of interest is the appearance of the percolation threshold in the spectra of an impurity, whose concentration, according to the quantitative spectral analysis, does not exceed 1 %. As follows from the results shown in Fig. 7, the temperature jump in the plasma volume leads to the change in the slope of the dependence for the intensity of sodium D-lines by approximately an order of magnitude. When the target composition changes, the effective brightness temperature, calculated by the line of Na, increases from 3000 K (below the threshold) to 4200 K (above the threshold). For emission at the resonance transition frequency, where the D-line self-reversal takes place, an even lower effective brightness temperature (2400 ± 200 K) is typical, which can be considered as the lowest boundary of the temperature layer containing sodium. The decrease in the emission spectrum intensity of sodium, observed for $x > 0.6$, requires additional investigation.

In the case of calcium, the dependence of the spectrum intensity on the target composition shows the same threshold behaviour, which is typical for the main components of the target. It is possible that calcium, forming stable compounds with silicon, such as Ca_2Si, CaSi and $CaSi_2$, proves to be in a bound state till the threshold and above it – in the atomic state.

Upon laser ablation of a binary silicon–silica mixture, nanostructures are produced more efficiently than in the case of the one-component target (see Figs 1 and 2). The dependences on the composition have three pronounced maxima. The maximum near $x = 0.33$, corresponding to the same density of silicon and oxygen atoms in plasma, can be related to the formation of fractal microscopic aggregate according to the model of two-dimensional percolation. The boundaries of inhomogeneities in the lase plume can serve as surfaces on which two-dimensional fractal structures are assembled [16]. Macroscopic fractal nanostructures (fractal shells [7]) are assembled in the boundary plume layer either directly from nanoclusters or two-dimensional and three-dimensional fractal microaggregates and take on the final form at temperatures close to the melting temperature. The range of target compositions in which macroshells are observed lies between the left and right maxima shown in Figs 1 and 2. It follows from the results of [8], where $Si_x(SiO_2)_{1-x}$ targets were ablated by nanosecond laser pulses, that in the plasma a three-dimensional percolation cluster is formed from silicon atoms for $x \sim 0.1$. Upon ablation by nanosecond pulses, the plasma temperature for all the compositions of the target exceeds 6000 K and SiO molecules are absent in its volume. When the target with a high content of silica is irradiated by millisecond pulses, the plasma temperature is ~ 3200 K and free silicon is absent in its volume. Therefore, we should expect that a percolation cluster is formed from molecules of silicon oxides [17]. It follows from Fig. 6 that the maximum concentration of oxygen and SiO molecules [according to (3)] takes place upon ablation of targets with $x \sim 0.1$.

5. Conclusions

The results of the study have shown that at a high pressure of the gas surrounding the target, the method of laser evaporation can be used to form efficiently two-dimensional and three-dimensional fractal nanostructures based on the percolation growth model. The dimensionality of the structures depends on the buffer gas pressure and the target composition. Near percolation thresholds the efficiency of nanostructure formation increases by an order of magnitude. Percolation takes place both in cooled and hot layers of the laser plasma, which is manifested in the formation of a fractal shell and threshold dependence of the intensity of discrete spectra of atoms of the target respectively. The dynamic nature of the percolation cluster at a high temperature allows one to consider it as a virtual gas-like low-dimensional structure. The study of the properties of this object, including its optical properties, is of great interest for further investigations.

Acknowledgements. This work was partially supported by the Russian Foundation for Basic Research (Grant No. 06-02-16812).

References

1. Marsen B., Sattler K. *Phys. Rev. B*, **60**, 11593 (1999).
2. Andrade J.S. Jr, Azevedo D.L., Correa Filho R., Costa Filho R.N. *Nano Lett.*, **5**, 1483 (2005).
3. Zhukhovitskii D.I. *Zh. Eksp. Teor. Fiz.*, **121**, 396 (2002).
4. Likal'ter A.A. *Usp. Fiz. Nauk*, **162**, 119 (1992) [*Physics-Uspekhi,* **35**, 591 (1992)].
5. Kask N.E., Michurin S.V., Fedorov G.M. *Kvantovaya Elektron.*, **34**, 524 (2004) [*Quantum Electron.*, **34**, 524 (2004)].
6. Kask N.E., Michurin S.V., Fedorov G.M. *Kvantovaya Elektron.*, **35**, 48 (2005) [*Quantum Electron.*, **35**, 48 (2005)].
7. Kask N.E., Leksina E.G., Michurin S.V., et al. *Kvantovaya Elektron.*, **32**, 437 (2002) [*Quantum Electron.*, **32**, 437 (2002)].
8. Kask N.E., Michurin S.V., Fedorov G.M. *Kvantovaya Elektron.*, **36**, 435 (2006) [*Quantum Electron.*, **36**, 435 (2006)].
9. Lee S.T., Wang N., Lee C.S. *Mater. Sci. Eng. A-Struct. Mater.,* **286**, 16 (2000).
10. Givargizov E.I. *Rost nitevidnykh i plastinchatykh kristallov iz para* (Growth of Whisker and Plate Crystals from Vapour) (Moscow: Nauka, 1977).
11. Landau L.D., Lifshits E.M. *Statistical Physics* (Oxford: Pergamon Press, 1980; Moscow: Nauka, 2002).
12. Toporov N.A., Barzakovskii V.P. *Vysokotemperaturnaya khimiya silikatnykh i drugikh oksidnykh system* (High-Temperature Chemistry of Silicate and Other Oxide Systems) (Moscow-Leningrad: Izd. of Acad. of Sciences of USSR, 1963).
13. *Termodinamicheskie svoistva individual'nykh veshchestv* (Thermodynamic Properties of Individual Materials) (Moscow: Nauka, 1982).
14. Wasserman A.A., Melosh H.J. *Proc. XXXIII Conf. 'Lunar and planetary science'* (Houston, 2002, No. 1308).
15. Kask N.E., Kornienko L.S., Fedorovich O.V. *Kvantovaya Elektron.*, **12**, 80 (1985) [*Sov. J. Quantum Electron.*, **15**, 44 (1985)].
16. Harilal S.S., Bindhu C.V., Tillack M.S., et al. *J. Appl. Phys.*, **93**, 2380 (2003).
17. Kieffer J., Angell C.A. *J. Non-Cryst. Sol.*, **106**, 336 (1988).